Rotating Spokes, Ionization Instability, and Electron Vortices in Partially Magnetized $E \times B$ Plasmas

Jean-Pierre Boeuf[1,*] and Masayuki Takahashi[2]
[1]Laplace, Université de Toulouse, CNRS, INPT, UPS, 118 Route de Narbonne, 31062 Toulouse, France
[2]Department of Aerospace Engineering, Tohoku University, Sendai 980-8579, Japan

(Received 24 January 2020; accepted 16 April 2020; published 8 May 2020)

Regions of enhanced light emission rotating in the azimuthal direction are present in various $\boldsymbol{E} \times \boldsymbol{B}$ plasma devices. A kinetic model reveals that these "rotating spokes" are due to electron heating and enhanced ionization localized along a double layer at the interface between a region of large electric field and a quasi-equipotential region close to the anode potential. Electrons drifting along this interface are heated due to ∇B drift in the large electric field region. The formation of electron vortices due to the velocity shear in the double layer also contributes to electron heating. The possibility for spoke motion in the retrograde $\boldsymbol{E} \times \boldsymbol{B}$ direction as well as in the $\boldsymbol{E} \times \boldsymbol{B}$ direction, observed experimentally, can be reproduced and explained.

DOI: 10.1103/PhysRevLett.124.185005

In plasma devices such as magnetrons [1] and Hall thrusters [2] an external magnetic field $\boldsymbol{B}$ is placed perpendicular to the applied electric field $\boldsymbol{E}$ to confine the electrons and allow ionization and plasma formation at low gas pressure. These devices are cylindrically symmetric, with $\boldsymbol{E} \times \boldsymbol{B}$ in the azimuthal direction to allow efficient electron confinement. In these "partially magnetized plasmas" electrons are strongly magnetized (electron Larmor radius ρ_e small with respect to the plasma size L, $\rho_e \ll L$) while ions are not ($\rho_i \gtrsim L$). Turbulence and instabilities resulting in anomalous transport and in the formation of coherent structures are present in partially magnetized $\boldsymbol{E} \times \boldsymbol{B}$ plasmas as in fusion or space plasmas but the physics of these instabilities is specific due to the difference in the magnetization of electrons and ions [3] and to the existence of localized ionization regions. An example of instability that has been thoroughly studied in the recent years is the electron cyclotron drift instability (ECDI), first identified in the context of collisionless shocks in space plasmas [4,5]. Particle-in-cell (PIC) simulations predict that the ECDI is present and controls electron transport in the exhaust region of Hall thrusters where a large axial electric field in the quasineutral plasma extracts and accelerates positive ions [6–9].

A longer wavelength instability, much easier to observe experimentally, is characterized by the rotation of a region of enhanced light emission ("rotating spoke") at relatively low velocities. Such moving macroscopic plasma nonuniformities have been reported in most $\boldsymbol{E} \times \boldsymbol{B}$ plasma devices. The first studies date back to the 1960s when rotating-plasma machines were investigated as possible devices for fusion applications [10]. The goal was to generate a large radial electric field E in the quasineutral plasma, for example in a coaxial electrode system with a strong axial magnetic field B. The plasma was expected to rotate at the velocity E/B. It was found experimentally that there was a maximum "burning voltage" of the discharge, i.e., a maximum plasma rotation velocity [11]. This limitation of the rotation velocity was attributed to an abnormal ionization mechanism [12] that was related to the concept of critical ionization velocity (CIV) introduced by Alfven [13]. In a model proposed by Piel, Möbius, and Himmel [14], the anomalous ionization was associated with the formation and rotation of an azimuthal double layer where electrons were heated by a two-stream instability. More recently, a PIC simulation [15,16] of a cylindrical magnetron discharge showed similarities with this model but the reason for the presence of the double layer was not elucidated and the question of the nature of electron heating in the double layer was not clarified.

Rotating spokes have also been observed in Hall thrusters [17–20] and in pulsed planar magnetrons used in plasma processing, high power impulse magnetron sputtering (HiPIMS) [1,21]. In some papers on Hall thrusters [17] or magnetrons [22] the CIV concept has been invoked to explain the presence of rotating spokes, but there is no consensus on the physics of the rotating spokes in spite of important recent progress in the diagnostic and qualitative interpretation of these phenomena [23,24]. An intriguing feature of experiments on $\boldsymbol{E} \times \boldsymbol{B}$ devices is that spokes do not always rotate in the $\boldsymbol{E} \times \boldsymbol{B}$ direction. Retrograde motion (in the $-\boldsymbol{E} \times \boldsymbol{B}$ direction) has also been observed in the low current regime of HiPIMS or in direct current (dc) magnetrons [23,24].

In this Letter we present simulations of a recently published experiment by Ito, Young, and Cappelli [25] on a simple dc magnetron discharge, where self-organized structures rotating in the $-\boldsymbol{E} \times \boldsymbol{B}$ direction were observed

with a high framing rate camera. On the basis of simulation results in conditions around this experiment, we propose a new insight into the physics of rotating spokes. This new model of the physics of rotating spokes shares some qualitative aspects with, but is clearly distinct from, the CIV model of Ref. [14].

The experiment of Ito, Young and Cappelli consists of a small planar dc magnetron discharge in argon (2 mm gap, pressure 20 Pa, magnetic field 1 T at cathode, 0.1 T at anode) where the light emission is observed with a fast camera through a transparent planar anode. The relatively large magnetic field and pressure are related to the small dimensions of the device and according to classical discharge scaling laws similar features should be observed for dimensions 10 times larger and magnetic field and pressure 10 times smaller.

The two-dimensional (2D) PIC-MCC model described in previous papers [15,16,26] has been used to simulate this experiment. The simulation domain is defined by the axial and azimuthal directions $\hat{x}$ and $\hat{y}$.

The axial cathode-anode distance is $d = 2$ mm, and the azimuthal length is $w = 4$ mm. Periodic boundary conditions are assumed in the azimuthal direction for the particle trajectories and for the electric potential. The magnetic field is perpendicular to the simulation domain and pointing inward as shown in Fig. 1. Its magnitude B varies axially according to $B(x) = a\exp(-x^2/2\sigma^2) + b$, with $\sigma = 0.35d$. a and b are chosen so that $B(0) = 1$ and $B(d) = 0.1$ T. The discharge is sustained by ionization (calculated self-consistently in the Monte Carlo module) and secondary electron emission at the cathode due to ion impact. The argon electron-neutral and ion-neutral scattering cross sections are the same as in Refs. [15,16]. An effective secondary emission coefficient γ is used in the simulation. The *net* flux Γ_e of electrons leaving the cathode is related to the ion flux Γ_i by $\Gamma_e = -\gamma\Gamma_i$, i.e., an electron coming back to the cathode is reemitted. $\gamma = 0.005$ is used in the simulations. Electrons are emitted according to a semi-Maxwellian distribution at a temperature $T_e = 2$ eV. The cathode is grounded and the anode voltage is set to $U_d = 260$ V. The simulations were started with a uniform plasma density $n_e = n_i = 2 \times 10^{16}$ m^{-3}. Most simulations were performed on a 128×256 grid with about 300 particles per cell at steady state (reached in less than 10 μs).

In these conditions the simulation predicts the formation of an ionization instability (region of enhanced ionization, or spoke) moving in the $-\boldsymbol{E} \times \boldsymbol{B}$ direction at a velocity close to 10 km/s. The calculated average current density is 300 A/m^2, not far from the current density of 10^3 A/m^2 deduced from the experiments. When the simulation is performed with an azimuthal dimension of 8 instead of 4 mm, two similar spokes are present in the simulation domain and move in the $-\boldsymbol{E} \times \boldsymbol{B}$ direction. These features (retrograde motion, spoke velocity, and periodicity) are in good agreement with the experiments of Ref. [25].

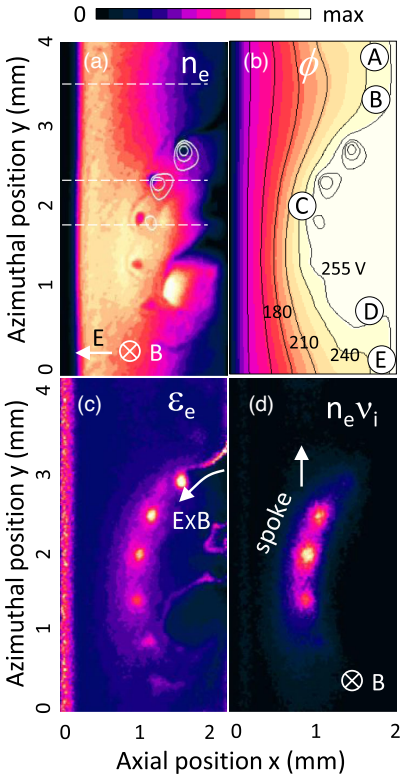

FIG. 1. Contours of constant (a) electron density, (b) plasma potential, (c) electron mean energy, and (d) ionization rate at a given time in the conditions described in the text, corresponding to the experiment of Ref. [25]. The maximum values are respectively 4×10^{17} m^{-3}, 267 V, 15 eV, 2×10^{25} m^{-3} s^{-1}. The spoke, plasma nonuniformity, and potential structure move together up in the $-\boldsymbol{E} \times \boldsymbol{B}$ direction at about 10 km/s while the electron vortices (local maxima in the electron temperature, potential, and ionization rate, and associated "holes" in the electron density) move down in the $\boldsymbol{E} \times \boldsymbol{B}$ direction at a velocity about 10 times larger. The potential contours above 255 V, shown in (b) and (a) are at 262, 264, and 266 V. Movies available in the Supplemental Material [27].

However, the physics of the simulated instability is not consistent with the theory of Ito *et al.* [25], one reason being that this theory cannot describe ionization instabilities.

Figure 1 shows the space distribution of the main plasma properties at a given time in the simulation at steady state. The plasma presents a strong azimuthal nonuniformity that creates a distortion of the equipotential lines. This distortion separates the plasma in two regions: one region of low electric field [lighter color region in Fig. 1(b)] whose potential is close to the anode potential and a region of large axial electric field between the cathode and the quasi-equipotential region.

A double layer is formed at the boundary between the two regions. We call this boundary [the ABCDE line in Fig. 1(b)] "the interface" in the following. Note that the electric field is perpendicular to the equipotential lines so that the $\boldsymbol{E} \times \boldsymbol{B}$ electron drift follows the equipotential

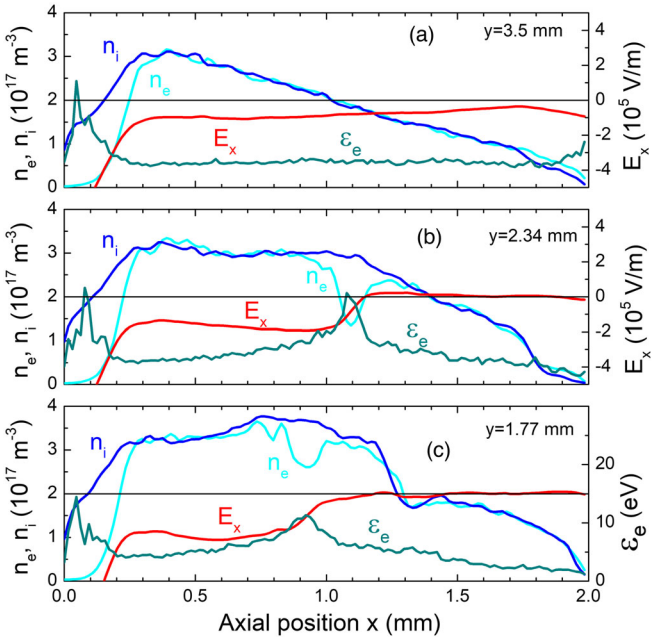

FIG. 2. Axial profiles of the electron density, ion density, axial electric field, and electron mean energy at different azimuthal positions indicated by the dashed lines in Fig. 1(a) and at the same time as Fig. 1. Same scale for E_x and ε_e in the three plots.

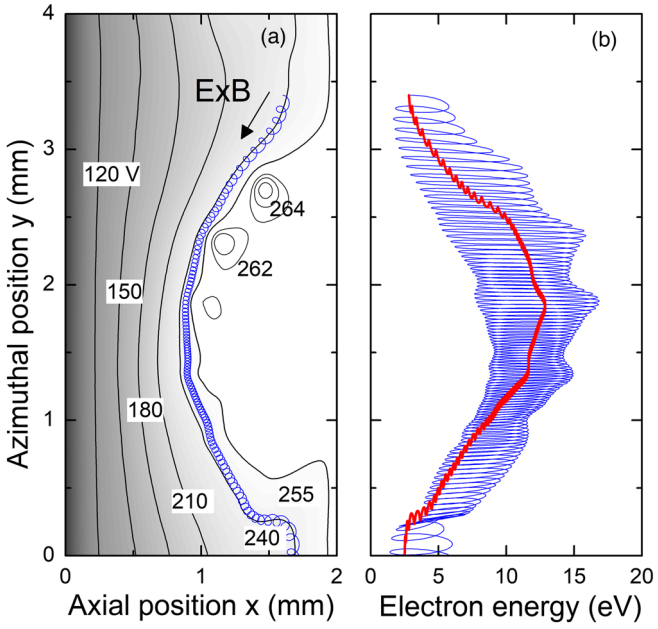

FIG. 3. (a) Equipotential contours, and example of electron trajectory at a given time (same conditions as Fig. 1), close to the double layer, on the left side of the BCD line of Fig. 1. (b) Variations of the electron energy along the same trajectory. The initial electron velocity, at $x = 1.6$ mm, $y = 3.4$ mm, is $v_x = 10^6$ m/s, $v_y = 0$. The red line is the average energy calculated assuming electron heating due to ∇B drift.

contours. The interface is close to the anode along the AB and DE segments and some electrons flow to the anode in these regions.

The formation of the double layer at the interface is the consequence of the electron deficit due to losses at the anode not being entirely balanced by ionization along this line. We see on Fig. 1(d) that ionization is enhanced along the interface and on the cathode side of the equipotential region (left side of the BC segment). It is interesting to note that in these conditions, most of the overall ionization takes place in this region, i.e., the plasma is sustained by the ionization instability. The breaking of quasineutrality in the double layer can be clearly seen in Fig. 2, which displays the axial profiles of the electron density, ion density, axial electric field, and electron temperature at the three azimuthal locations. Note that the sign of the axial electric field close to the anode in Fig. 2(a) is such that some electrons in the AB and DE regions can reach the anode through collisional transport parallel to the electric field.

One reason for the enhanced electron heating and ionization in the BC region is cross-field electron transport associated with the axial variations of the magnetic field (∇B drift [28]) in the large electric field region on the left of the BC line. This is illustrated in Fig. 3. This figure shows an example of electron trajectory [Fig. 3(a)] in the vicinity of the interface, on the left side of the BCD segment, and the variations of the electron energy over the same trajectory [Fig. 3(b)]. The mean value of the electron energy increases by about 5 eV when the electron moves parallel to BC (electron heating) in the spoke front and decreases when the electron moves parallel to CD (electron cooling). The consequence of the electron heating along BC is the intense ionization that takes place on the left side of the BC region in Fig. 1(d). The ∇B electron drift velocity is given by [28] $\boldsymbol{v}_{\nabla B} = -1/2\ \rho_e v_\perp \boldsymbol{B} \times \nabla B/B^2 = -\varepsilon_\perp \boldsymbol{B} \times \nabla B/B^3$, where $v_\perp$ is the electron velocity and $\varepsilon_\perp$ the electron energy in eV, perpendicular to the magnetic field. $\boldsymbol{v}_{\nabla B}$ is directed in the azimuthal direction downward. The electron heating or cooling is given by $\partial_t \varepsilon_\perp = -\boldsymbol{v}_{\nabla B}.\boldsymbol{E} = \varepsilon_\perp E_y/(BL)$, where $L = |B/\partial_x B|$. E_y is positive along BC and negative along CD so electron heating takes place along BC and electron cooling along CD. Note that this electron heating and cooling is consistent with conservation of the first adiabatic invariant $\varepsilon_\perp/B$ along a collisionless electron trajectory. The electron heating frequency $\alpha = E_y/(BL)$ can be as large as 10^9 s^{-1} in the vicinity and on the left side of the BC line ($E_y/B \approx 5 \times 10^5$ m/s and $L \approx 0.5$ mm) leading to significant heating (the electron transit time along BC is several ns). This simple estimation is confirmed numerically on Fig. 3(b), where the red line corresponds to the electron mean energy calculated by integrating the expression above along the electron trajectory: $\varepsilon_\perp = \varepsilon_{\perp 0} - \int \boldsymbol{v}_{\nabla B}.\boldsymbol{E} dt$.

The electric potential presents local maxima of several volts above the anode potential in the quasiequipotential region [Figs. 1(b), 3(a)]. These maxima are associated with the formation of electron vortices rotating around the

potential maxima, due to the electron velocity shear in the double layer. These vortices (apparent as electron density "holes" and local maxima of the electron mean energy and ionization rate in Fig. 1) move along the double layer at the local E/B velocity. The physics is similar to that of the diocotron instability observed in pure electron plasmas [29] except that the electron vortices form here in a local potential maximum rather than potential minimum, due to the positive space charge of the double layer. This is the reason why the vortices form "holes" instead of "clumps" [29] in the electron density, as can be seen in Fig. 1(a). The local maxima of the potential move with the electron hole vortices along the double layer (see Supplemental Material [27]) and this electron-wave interaction also contribute to electron heating as evidenced by the local maxima of the ionization rate around the electron vortices [Fig. 1(d)]. The physics of electron heating in the vortices needs further investigation. Electron heating due to ∇B drift is dominant in the conditions considered here and seems to be responsible for the stability of the spoke.

The reason for the spoke motion in the $-\boldsymbol{E}\times\boldsymbol{B}$ direction in the conditions of Fig. 1 can be understood simply by the fact that the ionization region is located on the side of the plasma and potential maxima that is opposite to the $\boldsymbol{E}\times\boldsymbol{B}$ direction. The plasma and ionization region (spoke) apparently "move" in the $-\boldsymbol{E}\times\boldsymbol{B}$ direction, i.e., in the region where new electrons and ions are generated by ionization. This is illustrated in Fig. 4(a). The question is now, why spoke rotation is also observed in the $\boldsymbol{E}\times\boldsymbol{B}$ direction in other experiments (HiPIMS [23,24]). We performed simulations in the same conditions as Fig. 1 but at a pressure of 0.1 torr instead of 0.15 torr, and with $B(0) = 0.5$ T instead of 1 T (the electron current density emitted by the cathode was imposed and equal to 2 A/m^2 in this simulation). In these conditions the simulations predict spoke rotation in the $+\boldsymbol{E}\times\boldsymbol{B}$ direction as illustrated in Fig. 4(b). The main differences between the two cases are (i) the position of the ionization region with respect to the plasma density, and (ii) the direction of the ion flow in the spoke front. In Fig. 4(a) new electrons and ions are generated in and above the location of maximum plasma density and ions are not expelled from the front by the electric field. In Fig. 4(b) ions are expelled azimuthally from the front faster than they are generated by ionization. This can be simply formulated by writing the ion continuity equation $\partial_t n_i = S - \nabla.n_i\boldsymbol{v_i}$ at the starting point of the arrows representing the ion flux in the spoke front in Fig. 4 (S is the ionization rate, $\boldsymbol{v_i}$ the ion mean velocity). In Fig. 4(a), $S > \nabla.n_i\boldsymbol{v_i}$ so $\partial_t n_i > 0$ and the front moves in the upward ($-\boldsymbol{E}\times\boldsymbol{B}$) direction. The opposite is true for Fig. 4(b). This is clearly illustrated by the color maps of $\partial_t n_i$ on top of Fig. 4. Note the sharp variation and sign reversal of $\partial_t n_i$ in Fig. 4(b), corresponding to the acceleration of ions out of the spoke front. This is similar to what is expected in the CIV concept.

The conditions of Fig. 4(b) are likely to be met when the azimuthal component of the electric field in the spoke front is larger than the axial component. In any case the simulation results indicate that the same physics is responsible of spoke rotation in the retrograde $\boldsymbol{E}\times\boldsymbol{B}$ direction as well as in the $\boldsymbol{E}\times\boldsymbol{B}$ direction.

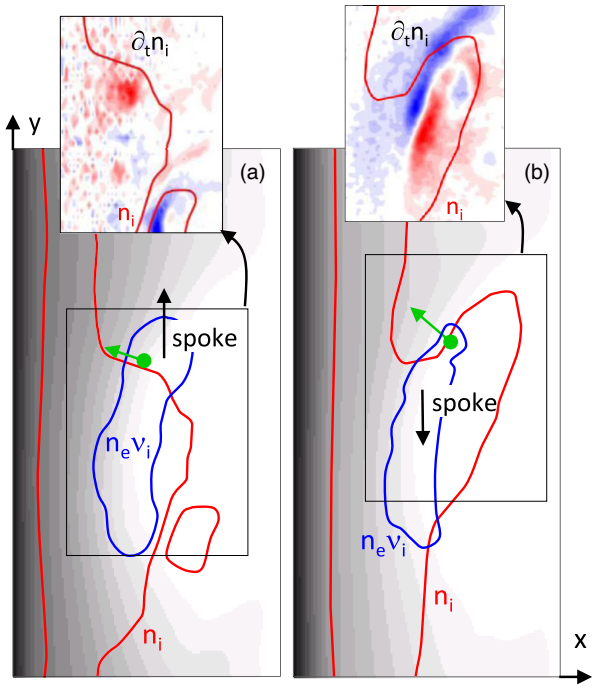

FIG. 4. Equipotential contours (gray), and lines of constant plasma density and ionization rate corresponding to 70% of their maximum values. The green arrows indicate the ion flux direction in the spoke front. (a) Spoke rotation in the $-\boldsymbol{E}\times\boldsymbol{B}$ direction, case of Fig. 1, (b) rotation in the $+\boldsymbol{E}\times\boldsymbol{B}$ direction, same conditions as Fig. 1 but at a pressure of 0.1 torr instead of 0.15 torr, and with $B(0) = 0.5$ T instead of 1 T. The red and blue color maps on top of the figure represent the space distributions of $\partial_t n_i$ in the spoke region (white to red color scale: $\partial_t n_i > 0$, white to blue color scale:$\partial_t n_i < 0$). Movies available in the Supplemental Material [27].

The main results can be summarized as follows. The small cross-field electron mobility is responsible for an instability (presumably of the Simon-Hoh type [3,26] in its initial phase) that leads to an azimuthal distortion of the plasma potential and density. This distortion allows some electrons to flow to the anode along an equipotential line connecting the cathode and anode regions.

A double layer is generated along this line by the drop in electron density due to electron losses to the anode along this line. Electrons gain energy due to ∇B induced cross-field transport while drifting along the double layer from anode region to cathode region. The formation of electron vortices due to the velocity shear in the double layer also contributes to electron heating. Ionization is enhanced in that region, leading to the formation of a spoke. The spoke can rotate in the $-\boldsymbol{E}\times\boldsymbol{B}$ as well as in the $+\boldsymbol{E}\times\boldsymbol{B}$ direction depending on the position of the plasma nonuniformity with respect to the ionization region and on the relative

values of the axial and azimuthal components of the electric field in the spoke.

The main similarities of the mechanism described above with the CIV model of Ref. [14] are the presence of a double layer at the spoke front and the enhanced electron heating and ionization in that region but the reason for the formation of a double layer, the mechanism of electron heating, and the spoke velocity are distinct from those invoked in the CIV model. Finally, we note that the conclusions of recent experiments [23,24] and of the present model are converging on a number of points: existence of a double layer at the spoke front, energization of electrons around the double layer, and possible rotation in the $\pm \boldsymbol{E} \times \boldsymbol{B}$ direction.

*Corresponding author.
jpb@laplace.univ-tlse.fr

[1] A. Anders, Reactive high power impulse magnetron sputtering (R-HiPIMS), J. Appl. Phys. **121**, 171101 (2017).
[2] J.-P. Boeuf, Tutorial: Physics and modeling of Hall thrusters, J. Appl. Phys. **121**, 011101 (2017).
[3] A. I. Smolyakov, O. Chapurin, W. Frias, I. Koshkarov, I. Romadanov, T. Tang, M. V. Umansky, Y. Raitses, I. Kaganovich, and V. P. Lakhin, Fluid theory and simulations of instabilities, turbulent transport and coherent structures in partially-magnetized plasmas of ExB discharges, Plasma Phys. Controlled Fusion **59**, 014041 (2017).
[4] D. Forslund, R. Morse, and C. Nielson, Electron Cyclotron Drift Instability, Phys. Rev. Lett. **25**, 1266 (1970).
[5] M. Lampe, W. M. Manheimer, J. B. McBride, J. H. Orens, R. Shanny, and R. N. Sudan, Nonlinear Development of the Beam-Cyclotron Instability, Phys. Rev. Lett. **26**, 1221 (1971).
[6] J. C. Adam, A. Héron, and G. Laval, Study of stationary plasma thrusters using two-dimensional fully kinetic simulations, Phys. Plasmas **11**, 295 (2004).
[7] J. Cavalier, N. Lemoine, G. Bonhomme, S. Tsikata, C. Honore, and D. Gresillon, Hall thruster plasma fluctuations identified as the ExB electron drift instability: Modeling and fitting on experimental data, Phys. Plasmas **20**, 082107 (2013).
[8] T. Lafleur, S. D. Baalrud, and P. Chabert, Theory for the anomalous electron transport in Hall effect thrusters. II. Kinetic model, Phys. Plasmas **23**, 053503 (2016).
[9] J. P. Boeuf and L. Garrigues, ExB electron drift instability in Hall thrusters: Particle-in-cell simulations vs. theory, Phys. Plasmas **25**, 061204 (2018).
[10] J. M. Wilcox, Review of high-temperature rotating-plasma experiments, Rev. Mod. Phys. **31**, 1045 (1959).
[11] U. V. Fahleson, Experiments with plasma moving through neutral gas, Phys. Fluids **4**, 123 (1961).
[12] G. Himmel and A. Piel, The velocity limitation in a rotating plasma device of the homopolar type, J. Phys. D **6**, L108 (1973).
[13] H. Alfven, *On the Origin of the Solar System* (Clarendon Press, Oxford, 1954).
[14] A. Piel, E. Möbius, and G. Himmel, The influence of the plasma inhomogneity on the critical velocity phenomenon, Astrophys. Space Sci. **72**, 211 (1980).
[15] J. P. Boeuf and B. Chaudhury, Rotating Instability in Low-Temperature Magnetized Plasmas, Phys. Rev. Lett. **111**, 155005 (2013).
[16] J. P. Boeuf, Rotating structures in low temperature magnetized plasmas - Insight from particle simulations, Front. Plasma Phys. **2**, 74 (2014).
[17] C. S. Janes and R. S. Lowder, Anomalous electron diffusion and ion acceleration in a lowdensity plasma, Phys. Fluids **9**, 1115 (1966).
[18] M. McDonald and A. D. Gallimore, Rotating spoke instabilities in hall thrusters, IEEE Trans. Plasma Sci. **39**, 2952 (2011).
[19] C. L. Ellison, Y. Raitses, and N. J. Fisch, Cross-field electron transport induced by a rotating spoke in a cylindrical Hall thruster, Phys. Plasmas **19**, 013503 (2012).
[20] M. J. Sekerak, B. W. Longmier, A. D. Gallimore, D. Brown, R. R. Hofer, and J. E. Polk, Azimuthal spoke propagation in hall effect thrusters, IEEE Trans. Plasma Sci. **43**, 72 (2015).
[21] N. Brenning, D. Lundin, T. Minea, C. Costin, and C. Vitelaru, Spokes and charged particle transport in HiPIMS magnetrons, J. Phys. D **46**, 084005 (2013).
[22] N. Brenning and D. Lundin, Alfvén's critical ionization velocity observed in high power impulse magnetron sputtering discharges, Phys. Plasmas **19**, 093505 (2012).
[23] M. Panjan and A. Anders, Plasma potential of a moving ionization zone in DC magnetron sputtering, J. Appl. Phys. **121**, 063302 (2017).
[24] A. Hecimovic and A. von Keudell, Spokes in high power impulse magnetron sputtering plasmas, J. Phys. D **51**, 453001 (2018).
[25] T. Ito, C. V. Young, and M. A. Cappelli, Self-organization in planar magnetron microdischarge plasmas, Appl. Phys. Lett. **106**, 254104 (2015).
[26] J. P. Boeuf, Micro instabilities and rotating spokes in the near-anode region of partially magnetized plasmas, Phys. Plasmas **26**, 072113 (2019).
[27] See Supplemental Material at http://link.aps.org/supplemental/10.1103/PhysRevLett.124.185005 for movies showing the time evolution of the plasma properties for the rotating spokes of Figs. 1 and 4.
[28] F. F. Chen, *Introduction to Plasma Physics and Controlled Fusion* (Plenum Press, New York, 1984).
[29] A. Kabantsev, C. F. Driscoll, D. H. E. Dubin, and D. A. Schecter, Experiments and theory on 2D electron vortex dynamics in sheared flows, J. Plasma Fusion Res. Ser. **4**, 117 (2001).